Swinburne Research Bank

http://researchbank.swinburne.edu.au

The Las Campanas/AAT Rich Cluster Survey I: Precision and Reliability of the Photometric Catalogue

Kevin A. Pimbblet,[1] Ian Smail,[1] Alastair C. Edge,[1] Warrick J. Couch,[2]
Eileen O'Hely,[2] and Ann I. Zabludoff.[3]

[1] *Department of Physics, University of Durham, South Road, Durham, DH1 3LE, UK*
[2] *School of Physics, University of New South Wales, Sydney, NSW 2052, Australia*
[3] *Steward Observatory, University of Arizona, Tucson, 85721, USA*

1 February 2008

ABSTRACT

The Las Campanas Observatory and Anglo–Australian Telescope Rich Cluster Survey (LARCS) is a panoramic imaging and spectroscopic survey of an X-ray luminosity-selected sample of 21 clusters of galaxies at $0.07 < z < 0.16$. CCD imaging was obtained in B and R of typically 2-degree wide regions centred on the 21 clusters, and the galaxy sample selected from the imaging is being used for an on-going spectroscopic survey of the clusters with the 2dF spectrograph on the Anglo-Australian Telescope. This paper presents the reduction of the imaging data and the photometric analysis used in the survey. Based on an overlapping area of 12.3 square degrees, we compare the CCD-based LARCS catalogue with the photographic-based galaxy catalogue used for the input to the 2dF Galaxy Redshift Survey (2dFGRS) from the Automated Plate Measuring Machine(APM) to the completeness of the GRS/APM catalogue, $b_J = 19.45$. This comparison confirms the reliability of the photometry across our mosaics and between the clusters in our survey. This comparison also provides useful information about the properties of the GRS/APM. The stellar contamination in the GRS/APM galaxy catalogue is confirmed to be around 5–10 percent, as originally estimated. However, using the superior sensitivity and spatial resolution in the LARCS survey we find evidence for four distinct populations of galaxies that are systematically omitted from the GRS/APM catalogue. The characteristics of the 'missing' galaxy populations are described, reasons for their absence examined and the impact they will have on the conclusions drawn from the 2dF Galaxy Redshift Survey are discussed.

Key words: surveys, catalogues, galaxies: photometry

1 INTRODUCTION

Panoramic surveys based upon systematic photographic imaging of large areas of the sky have under-pinned a large fraction of astrophysical research since the 1950s, with the three main Schmidt telescopes, at Palomar, Siding Springs and La Silla, completing at least 14 major surveys over this period. The full exploitation of these observations has been achieved through the digitization of the photographic plates on facilities such as the Automated Plate Measuring Machine (APM, Kibblewhite et al. 1984) at Cambridge, or COSMOS at Edinburgh (MacGillivray & Stobie, 1984).

While they cover impressively large areas, the photographic surveys have several drawbacks which makes them unsuitable for some applications. In particular, the low sensitivity and non-linear response of standard photographic plates means that the surveys have relatively bright surface brightness limits and require significant effort to reliably calibrate the magnitude scale over the whole range detected. Indeed repeated scans of individual plates using the measuring machines suggests a scatter in the measured magnitudes for sources of at least ~ 0.04 mags (Maddox et al. 1990a), before other contributions are included. The relatively poor spatial resolution achieved on the Schmidt plates also limits the reliability of star–galaxy separation, placing additional restrictions on the questions which can be addressed with these data.

Panoramic imaging surveys using CCDs circumvent many of the drawbacks of photographic surveys by virtue of their high quantum efficiency and good linearity of CCD devices. Large format CCDs (and mosaic cameras) are therefore now being used to undertake wide-field surveys, whose depth, resolution and photometric precision far exceeds those achieved using photographic plates.

This paper describes one such project – the Las Campanas/AAT Rich Cluster Survey (LARCS). LARCS is a long-term project to study a statistically-reliable sample of the most luminous X-ray clusters at intermediate redshifts ($z = 0.07$–0.16) in the southern hemisphere. The goals of the project are to understand the influence of environment on the characteristics of galaxies, such as luminosity, star formation history and morphology. To achieve this we map the photometric, spectroscopic and dynamical properties of galaxies in rich cluster environments at $z \sim 0.1$, tracing the variation in these properties from the high-density cluster cores out into the surrounding low-density field, beyond the turn-around radius ($\gtrsim 10\,\mathrm{Mpc}$)[⋆]. For the most massive clusters at $z \sim 0.1$, the turn-around radius corresponds to roughly 1 degree and therefore we require panoramic CCD imaging covering 2-degree diameter fields, as well as spectroscopic coverage of similar fields. The former is achieved by mosaicing CCD images from the 1-m Swope telescope at Las Campanas Observatory, while the latter comes from the subsequent spectroscopic follow-up with the 400-fibre 2dF multi-object spectrograph on the 3.9-m Anglo-Australian Telescope (AAT).

To ensure that the results from the survey can be reliably compared to theoretical models, well-defined selection criteria are used to identify the cluster sample used. The LARCS sample is selected from the X-ray brightest Abell Clusters (XBACs) catalogue of Ebeling et al. (1996) constructed from the *ROSAT* All-Sky Survey. XBACs is an all-sky, X-ray flux limited, sample of 242 Abell clusters and is effectively a complete sample of richest clusters at $z \lesssim 0.16$ (Ebeling et al. 1996). We therefore restrict our sample to the most X-ray luminous ($L_X \geq 3.7 \times 10^{44}\,\mathrm{erg\,s^{-1}}$) southern clusters (with $\delta \leq 10\,\mathrm{deg}$, so accessible from the AAT) lying in the redshift range $0.07 \leq z \leq 0.16$. These selection criteria result in 53 clusters in the XBACs sample and from these a random subsample of 21 is selected for our survey. LARCS has a sufficiently large sample that it should provide a statistically-reliable view of the properties of both the cluster galaxies and how these relate to the characteristics of the clusters themselves. A summary of the 21 galaxy clusters is presented in Table 1, together with the current state of observations made.

The project has completed panoramic (2×2 degree^2) B and R broad-band imaging of the cluster sample from the 1-m Swope telescope at Las Campanas Observatory, Chile, totaling over 70 square degrees of sky (O'Hely et al. 1998, O'Hely 2000). These images are used to select galaxies for the on-going spectroscopic survey using 2dF. The final goal is to obtain spectra for roughly 20,000 galaxies in the 21 clusters providing an unprecedented view of the dynamics of rich clusters and their galaxy populations within a region encompassing the core, halo and in-fall regions of the clusters.

This paper presents the details of the photometric reduction, calibration and analysis of the CCD imaging used in LARCS. In addition, as a test of the LARCS catalogues we compare our catalogues in the fields of four clusters that overlap with the plate-based galaxy catalogue from the

APM, (Maddox et al. 1990a, 1990b) which is the basis of the 2dF Galaxy Redshift Survey (2dFGRS, Colless et al. 1998; Maddox et al. 1998).

The plan of the paper is as follows: In §2 we discuss the imaging observations obtained for our survey, data reduction methods and quality tests. We test both the photometric properties and the star-galaxy separation of our catalogues. In §3 we compare the galaxy catalogues derived from our CCD imaging with those from the photographic APM catalogue used by the 2dFGRS (referred to as the GRS/APM catalogue in the following). §4 deals with the properties of the galaxy populations which are missing from the GRS/APM catalogue – including both compact, high surface brightness galaxies and lower surface-brightness galaxies, examining their magnitude, spatial and colour distributions. We summarize our main conclusions in §5.

2   IMAGING OBSERVATIONS, REDUCTION AND ANALYSIS

Analysis of the clusters is based upon panoramic CCD imaging from the 1-m Swope telescope. High quality broad-band B and R CCD images of all the cluster were obtained over the course of three years, 1996–1998. These observations are summized in Table 1. The observations employed a thinned 2048×2048, $24\mu\mathrm{m}$ pixel Tektronics CCD giving a pixel scale of $0.696''$/pixel and a field of view for each exposure of $23.76' \times 23.76'$. With $44''$ overlaps the total coverage of the 5×5 mosaic of pointings is $\sim 2\,\mathrm{degrees}$ diameter (the corners of the mosaic are omitted to give a total of 21 pointings per cluster). The total exposure time per pointing is 500 s in B and 400 s in R, each split into two spatially-offset subexposures to facilitate cosmic-ray rejection and the removal of a small number of cosmetic features.

Here we have chosen to discuss in detail our optical analysis of four of the clusters: Abell 22, 1084, 1650 and 1651, which are also included within the region surveyed by the 2dFGRS. These clusters were observed in two runs: March 16th to 22nd 1996 and August 19th to 21st 1996. The details of these observations are in Table 2.

The imaging data are reduced in a standard manner using packages within IRAF, steps undertaken include debiasing, preliminary flatfielding with twilight flats, creation of super-flats from independent stacks of the science frames and the application of these to the science frames, alignment and co-addition of data using a cosmic-ray reject algorithm. The accuracy of the alignment is better than one pixel in all cases.

To test the precision of the flatfielding, the IRAF task IMSTAT is used to obtain the mean background levels at various locations on each mosaic tile. The variation in the sky background is found to be ≤ 1 percent in all cases.

Before constructing the object catalogues it is necessary to match the seeing of the B and R-band tiles so that reliable aperture colours could be measured. The matching is achieved by degrading the tile with the better seeing to that of the worse. A first pass of SExtractor (Bertin & Arnouts 1996) is used to obtain a rough list of stellar sources on the R-band tiles, by taking objects with CLASS_STAR > 0.9 (see §2.3). The seeing of the B and R tiles is estimated from the median value of the FWHM of these sources measured with

---

[⋆] Throughout this work values of $H_0 = 50h$ km s^{-1} Mpc^{-1} and $q_o = 0.5$ have been adopted.

Table 1. The 21 clusters in the LARCS sample and the multiwavelength observations so far obtained. The column headed 'Passbands' indicates the broad band filters used to observe each cluster. Other observations indicate *ROSAT* imaging (with the *PSPC* or *HRI* instruments), *XMM-Newton EPIC* time that has been allocated and observations undertaken with the 2dF spectrograph at the AAT.

Cluster	R.A. (J2000)	Dec.	z	L_X (erg s^{-1})	Passbands	Diameter (deg.)	Other Observations
A22	00 20 38.64	−25 43 19	0.131	5.31	B/R	2.0	2dF
A550	05 52 51.84	−21 03 54	0.125	7.06	B/R	2.0	
A644	08 17 25.20	−07 31 41	0.071	7.92	B/R	2.0	*PSPC, HRI, EPIC*
A1084	10 44 30.72	−07 05 02	0.134	7.42	B/R	2.0	*EPIC*
A1285	11 30 20.64	−14 34 30	0.106	5.47	B/R	2.0	
A1437	12 00 25.44	+03 21 04	0.133	7.72	B/R	2.0	*HRI*
A1650	12 58 41.76	−01 45 22	0.084	7.81	B/R	2.0	*HRI*
A1651	12 59 24.00	−04 11 20	0.084	8.25	B/R	2.0	*PSPC*
A1664	13 03 44.16	−24 15 22	0.127	5.36	B/R	2.0	*PSPC, HRI*
A2055	15 18 41.28	+06 12 40	0.102	4.78	B/R	2.0	*HRI, EPIC*, 2dF
A2104	15 40 06.48	−03 18 22	0.155	7.89	B/R	2.0	*PSPC, EPIC*, 2dF
A2204	16 32 46.80	+05 34 26	0.152	20.58	B/R	2.0	*PSPC*, 2dF
A2597	23 25 16.56	−12 07 26	0.085	7.97	B/R	2.0	*PSPC, HRI*
A3112	03 17 56.40	−44 14 17	0.070	7.70	B/R	2.0	*PSPC*
A3378	06 05 52.80	−35 18 04	0.141	6.87	B/R	2.0	*HRI*
A3888	22 34 32.88	−37 43 59	0.151	14.52	B/R	2.0	*PSPC, EPIC*, 2dF
A3921	22 49 59.76	−64 25 52	0.095	5.40	B/R	2.0	*PSPC*, 2dF
A2811	00 42 07.92	−28 32 10	0.108	5.43	$U/B/R/K$	0.6	*HRI*
A2345	21 26 58.56	−12 08 28	0.176	9.93	$U/B/R/K$	0.6	*HRI, EPIC*
A3814	21 49 06.48	−30 41 53	0.117	3.85	$U/B/R/K$	0.6	*HRI*
A2496	22 50 55.92	−16 23 35	0.122	3.71	$U/B/R/K$	0.6	*HRI*

Table 2. Log of LCO imaging observations made for the four clusters used in this work.

Cluster	Date (1996)	Passband	N(point)	Seeing (″)	Photometric?
Abell 22	Aug 20	R	3	1.0–1.1	yes
	Aug 21	R	6	1.1–1.3	yes
	Aug 22	R	12	1.0–1.4	yes
	Aug 21	B	15	1.0–1.1	yes
	Aug 22	B	6	1.0–1.1	yes
Abell 1084	Mar 20	R	10	1.1–1.8	no
	Mar 21	R	11	1.0–1.2	partial
	Mar 17	B	10	1.4–1.9	yes
	Mar 18	B	11	1.1–2.1	yes
Abell 1650	Mar 20	R	21	1.0–1.2	partial
	Mar 16	B	15	1.1–1.7	yes
	Mar 22	B	6	1.2–2.3	yes
Abell 1651	Mar 21	R	21	1.0–1.1	partial
	Mar 17	B	21	1.1–1.4	yes

the IMEXAMINE task. An initial estimate of σ, the value used to convolve the better seeing tile (typically the R-band images) to the worse one, is made and applied using the GAUSS task to create a new, degraded tile. The median seeing for the stars on the degraded tile is then measured using IMEXAMINE. The process is repeated iteratively to determine the correct value for σ (within the 1-σ scatter of the median FWHM) to match the seeing on the two tiles. Before convolution, differences of up to $1''$ may be present between the median FWHM of the R- and B-band tiles. After convolution the difference between the median seeing is $\lesssim 0.1''$ and colours can be reliably measured.

SExtractor is used to automatically analyse the tiles, detect sources and parametrize them. We catalogue the R-band frames, detecting sources having more than 12 contiguous pixels each 3σ of the sky above the background, equivalent to $\mu_R \sim 23.3$ mag. arcsec^{-2}. The resulting catalogues have 5σ detection limits for galaxies of $R = 21.1$–21.3. Spurious sources, such as satellite trails and diffraction spikes from bright stars, are cleaned manually from the resultant catalogues by visual inspection.

To derive colours for these sources PHOT within IRAF is used and colours are measured in $4''$ diameter apertures (typically $\sim 10\,\mathrm{kpc}$ at the cluster redshifts) from the seeing-matched frames. These colours are used in the following analysis to convert the R-selected sample to B-band to compare to the GRS/APM.

2.1 Photometry

The science frames are calibrated from the observations of standard stars selected from Landolt (1992), interspersed throughout each night. Typically we observed over 100 standard stars each night in each broad-band filter throughout the observing runs. We fit for colour terms each night from observations of the standards taken at the same airmass. Extinction is accounted for by fitting to the variation with airmass of the standard stars photometry in one night. On photometric nights, the variation in extinction coefficient and colour term are all within 1σ of each other. The photometric solutions for the photometric nights (Table 2) are typically accurate to better than 0.03 mags.

As some of the observations are made in non-photometric conditions it is necessary to independently calibrate such pointings. To achieve this, the photometry of sources appearing in the $44''$ inter-tile overlap regions is used to determine the magnitude offset between the non-photometric and photometric tiles in each passband. Only those sources which are unsaturated, not heavily blended or close to the chip's edge are used to obtain these values. To optimally employ magnitude offset information across the whole mosaic we use the method of Glazebrook (1994, G94). Using a single step algorithm, G94 generates appropriate magnitude offsets to be applied to the non-photometric tiles, whilst keeping the zero-points of the photometric tiles fixed. After application of G94 we estimate that the typical tile to tile variation in zero-points is $\leq 0.006\,\mathrm{mags}$, as estimated from the scatter in the magnitude offsets from the duplicated sources in the overlapping regions. The maximum deviations between tiles is $\sim 0.015\,\mathrm{mags}$. The photometric zeropoint errors of 0.03 mags are the dominant ones and the tile-to-tile variation in zero-points is small by comparison.

Figure 1 shows the zeropoint offsets between each pointing of an example (non-photometric) mosaic as a grey-scale before and after correction using the G94 algorithm. After calibration the entire mosaic is close to uniform, with a tile-to-tile rms of only 0.005 mags.

Once both passbands are calibrated, the final catalogue is constructed by combining the catalogues for the individual 21 tiles across the entire mosaic. Duplicate sources (from the overlapping regions) are removed by averaging their critical SExtractor parameters (e.g. total magnitude).

2.2 Astrometry

Astrometry is performed individually on each pointing of the mosaic. Approximately 60 bright ($B < 18.0$) stars per pointing are tied to the positions from the APM (http://www.ast.cam.ac.uk/apm/). The positions of the rest of the sources (galaxies and uncatalogued stars) are then obtained using the ASTROM package. As a quality test, we compare the astrometrical solution of sources within the $44''$ overlap regions of the 2 degree mosaics. Our internal accuracy is found to be better than $\leq 0.3''$, adequate for the needs of spectroscopy on 2dF.

2.3 Star–Galaxy Separation

Accurate star–galaxy separation is essential in extragalactic surveys. Robust separation is vital for minimizing stellar contamination, while at the same time retaining compact galaxies and optimising the efficiency of spectroscopic follow-up of the survey.

Following Reid et al. (1996) we construct a plot of the magnitude difference between $4.0''$ and $2.0''$ diameter apertures ($\Delta_{2''-4''}$) on the B-band exposures versus total B magnitude (Fig. 2). In such a diagram, stars should trace a horizontal locus due to their fixed profile shape (the telescope PSF) and therefore a fixed proportion of light in the two apertures. The horizontal sequence is seen in Figure 2 at $\Delta_{2''-4''} \sim 0.1$. Galaxies, which exhibit a range of more extended profile shapes, will show a wider range of $\Delta_{2''-4''}$ values. Close to the completeness limit of the frames, the galaxy and star loci overlap due to low signal-to-noise. Examination of Fig. 2 reveals that our CCD imaging can readily differentiate stars from galaxies down to a magnitude of at least $B \sim 20.5$.

We examine the potential of four further SExtractor parameters for usage in star–galaxy separation. Ellipticity is obtained from SExtractor's estimates of the semi-major and semi-minor axes for sources. The CLASS_STAR parameter (P^*) is SExtractor's own estimate of stellarity and uses shape information fed into a neural-network classifier that has been trained a priori on other images. Finally, we use two estimates of the compactness of the image profile: the concentration index (Abrahams et al. 1993) and FWHM. Plotted in Figure 3 are these critical parameters for both stars and galaxies from Abell 22. The other clusters follow the same distribution of sources on these planes. For the ellipticity and concentration index, the stars and galaxies, as defined with the $\Delta_{2''-4''}$ cut, overlap somewhat, whilst the converse is true for P^* and the FWHM measurements. Therefore both the FWHM and P^* are useful in differentiating stars and galaxies.

Three criteria are used to generate a robust and stringent definition of galaxies: $\Delta_{2''-4''} > 0.2$, FWHM > 2" and $P^* < 0.1$. In adopting these criteria, we must accept that a small number of stars and galaxies will be mis-classified. However, as demonstrated in Figures 2 and 3, the number of stellar sources fulfilling these rigorous criteria is small, ≤ 3 percent.

3 COMPARISON OF THE GRS/APM GALAXY CATALOGUE WITH LARCS

To test the reliability of the LARCS cataloging, photometry and star–galaxy separation, we now compare our sample to the galaxy catalogue from the APM survey, which is used by the GRS/APM.

The APM survey (Maddox et al. 1990a, 1990b) is constructed from photographic plate materials taken at the UK Schmidt Telescope Unit in Australia. Approximately 390 photographic IIIa-J plates are scanned by the APM. The
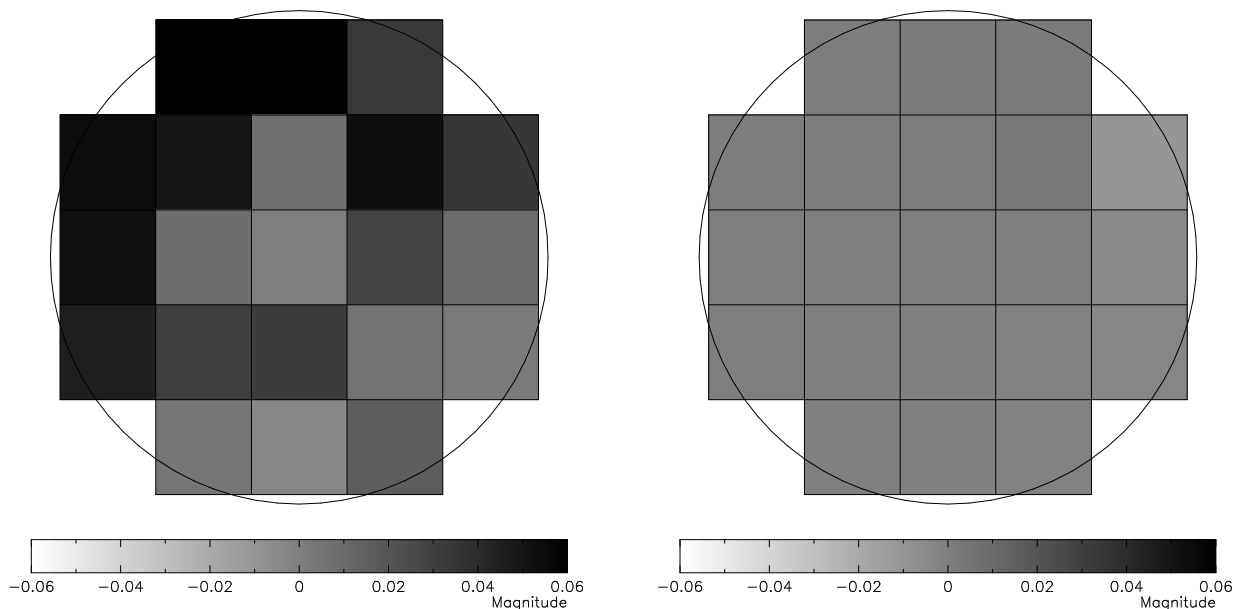
Figure 1. Left– Grey-scale of the zeropoint offsets between the different tiles within the R-band mosaic of Abell 1651. The range of offsets is given by the scale at the bottom. The mosaic is non-photometric and shows a range of over 0.06 magnitudes across the mosaic and an rms of 0.02. The circle has a diameter representing 2 degrees on the sky. Right– The same field after application of the iterative corrections from Glazebrook (1994) – the tile-to-tile rms is now reduced to ≤ 0.005 mag.
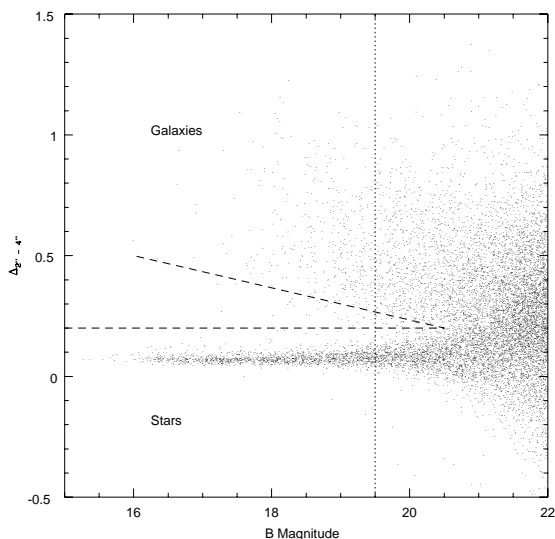

Figure 2. Difference between the 2.0″ and 4.0″ aperture magnitudes ($\Delta_{2''-4''}$) versus total magnitudes for all 31,851 sources within the LARCS Abell 22 catalogue. The stellar sources are those with $\Delta_{2''-4''} \sim 0.1$–0.2. Galaxies typically show larger values of $\Delta_{2''-4''}$. Our CCD imaging readily differentiates between stars and galaxies down to $B \sim 20.5$, beyond the magnitude limit of the GRS/APM catalogue. For the analysis of star-galaxy separation we use those sources brighter than $B = 19.5$. Those with $\Delta_{2''-4''} < 0.2$ are defined as stellar.

APM scans uses a 16-μm pixel with a sampling rate that produces a 0.54″ pixel scale. Magnitudes are defined using the Kodak emulsion in combination with a GG395 filter and zeropointed with Johnson B-band CCD photometry. The rms

random error in each galaxy magnitude is 0.1–0.2 mags to a depth of $b_J = 20.5$ (Maddox et al. 1990a). Subsequent field corrections are applied to the APM catalogues to account for non-photometric observations, vignetting and differential desensitization. Maddox et al. (1990b) argue that the rms plate zero-point error in the final matched survey catalogue is 0.04 mags. Objects in the overlapping regions between the plates are utilized for establishing the plate-to-plate variation and the zeropoints are iteratively corrected to remove these offsets.

Image surface brightness profiles are used in the APM to achieve star-galaxy separation. The residual differences between a given image profile and a stellar profile at the same magnitude are calculated, resulting in brighter stars being readily identified. At fainter magnitudes, the lower signal-to-noise in the images makes robust separation impossible. Maddox et al. (1990a) estimate that the catalogue's completeness is ~ 98 percent for $b_J < 19.5$, with a stellar contamination rate of 5–10 percent at the same depth depending upon proximity to the galactic plane.

The 2dFGRS is an ambitious project to collect high quality redshifts and spectra for $\sim 250,000$ galaxies brighter than $b_J = 19.45$ (extinction corrected). Galaxies are robustly selected from the extended version of the APM galaxy catalogue (Maddox et al. 1990a) covering a region of over 1700 square degrees in both the Northern and Southern Pole regions and used as the input to the 2dFGRS (Colless et al. 1998; Maddox et al. 1998; Folkes et al. 1999).

Of the LARCS clusters, four overlap with the 2dFGRS parent catalogue from the APM. The details of these cluster catalogues (Abell 22, 1084, 1650 and 1651) are presented in Table 3. The 0.3″ accuracy within the LARCS astrometry is more than adequate for identifying source matches with the APM catalogues.
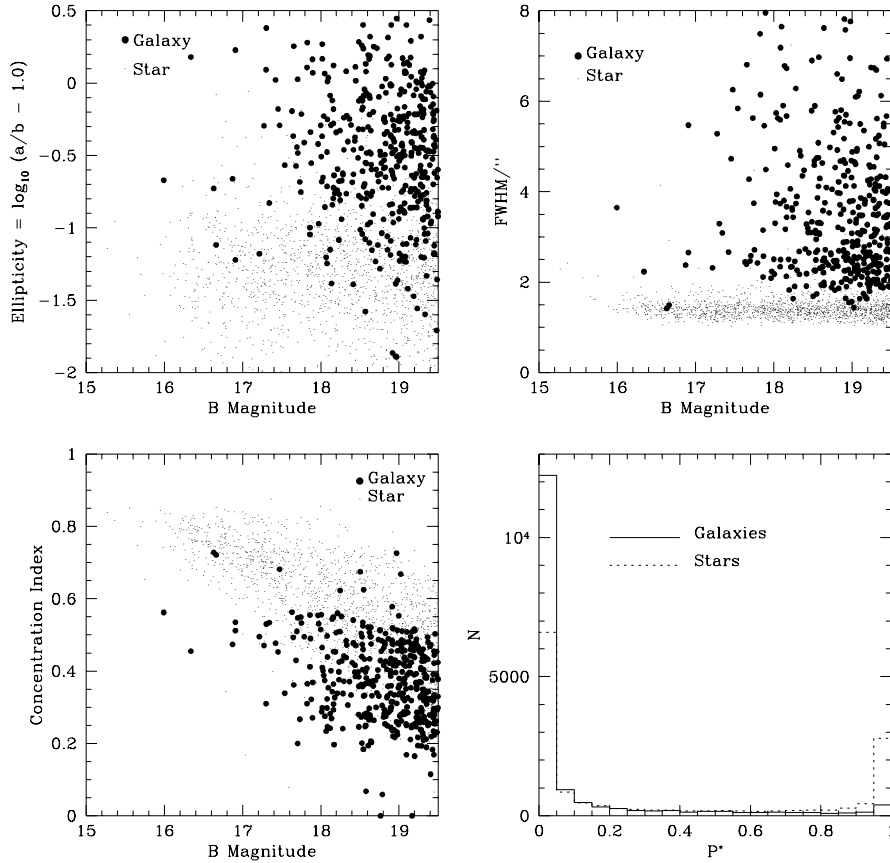
Figure 3. Plots of critical SExtractor parameters for stars and galaxies as defined from Figure 2. Upper Left: Ellipticity of the sources (defined as the ratio of semi-major to semi-minor axes) as a function of total magnitude. Upper Right: FWHM as a function of total magnitude. Lower Left: Concentration index as a function of total magnitude. Lower Right: Histogram of P^*, SExtractor's own probability of a given source being a star.

Table 3. Parameters of the LARCS clusters that overlap with the GRS/APM, including the number of sources catalogued in the LARCS CCD frames, the number of galaxies (defined using the criteria presented in §2.3) and the galactic cap region of the GRS/APM with which they overlap (Southern Galactic Pole, SGP; Northern Galactic Pole, NGP).

Cluster	N(Objects)	N(Galaxies)	Overlap
Abell 22	31851	15429	SGP
Abell 1084	37801	14494	NGP
Abell 1650	34403	13480	NGP
Abell 1651	42286	15801	NGP

3.1 Matching LARCS to GRS/APM

Here, we compare the GRS/APM catalogue down to the 2dFGRS magnitude cut-off of $b_J = 19.45$ (extinction corrected) across the LARCS/GRS overlap area of 12.3 square degrees.

The APM catalogue is divided into two distinct areas: Northern and Southern Galactic Pole regions. There are 2754 GRS/APM galaxies in the overlap of the GRS/APM with the four clusters in Table 3. One of the clusters (Abell 22) lies in the Southern Galactic Pole Region, whilst the other three overlapping clusters are in the Northern Galactic Pole Region.

The GRS/APM galaxy catalogue is matched to the full LARCS catalogues using a search radius of $3''$. Virtually all sources (~ 95 percent) in the GRS/APM have corresponding matches within LARCS. Those sources for which matches are not found are all visually inspected–their APM positions are over-plotted upon the corresponding LARCS mosaic pointings. In most cases the unmatched sources result from differences in blending and deblending of close sources between the two surveys. Most are resolved in the LARCS CCD imaging, whereas the APM sources appear as a blend of a number (typically 2–3) of LARCS sources (both galaxy-galaxy and galaxy-star blends). The centroiding for the astrometric solution is thus affected, resulting in the source lying outside the $3''$ search radius. Only three sources are found within the GRS/APM catalogue that do not have any likely counterpart in the LARCS imaging. These very rare sources (< 0.1 percent) are examples of APM mis-

Table 4. Comparison between the input GRS/APM catalogue and the four full LARCS catalogues. N(Matched) is the number of GRS/APM sources that are matched to LARCS. N(Galaxies) is the number of sources that we define as galaxies using the criteria presented in §3. N(Close blends) is the number of galaxies that the LARCS survey detects that are blended or in close proximity to a secondary source, which affects the astrometric matching routine. N(APM noise) is the number of sources existing within the GRS/APM survey that have no likely counterparts within LARCS – they are random detections, perhaps a moving source, plate flaw or a diffraction spike of a star.

Cluster	N(GRS/APM)	N(Matched)	N(Galaxies)	N(Close blends)	N(APM noise)
Abell 22	634	611	553	23	0
Abell 1084	473	463	371	10	0
Abell 1650	681	630	518	48	3
Abell 1651	966	932	752	34	0

detections perhaps caused by plate flaws or moving/variable sources. Table 4 summarizes the results of the matches with the total number of sources within each catalogue.

We further investigate the nature of the GRS/APM sources that are matched using the star–galaxy separation criteria of LARCS as presented in §2. The number of matched sources which satisfy all of the 'LARCS galaxy criteria' are presented in Table 4. Broadly 80 percent of matched sources defined as galaxies by the GRS/APM are also classified as galaxies by LARCS. We note that 80 percent is the *lower* limit of the number of galaxies as our galaxy determination is very strict.

We are also able to place a lower limit on the stellar contamination by inverting the star-galaxy selection criteria discussed previously. Conservatively, stars can be defined as having $\Delta_{2''-4''} < 0.2$, FWHM < 2.0" and $P^* > 0.9$. Of the matched GRS/APM galaxies, 3 percent are defined as stars by LARCS. Therefore at minimum, the stellar contamination of the APM is 3 percent, whilst at maximum it is 20 percent. Our result is close to the original estimation of 5–10 percent stellar contamination by Maddox et al. (1990a).

3.2 Photometric comparison

In this section we examine the magnitudes of sources in the LARCS and GRS/APM catalogues–searching for zero-point differences between the four cluster fields, as well as between the Northern and Southern Galactic Pole regions of the GRS/APM.

To undertake such a comparison, one must convert LARCS' R-selected sample to the b_J system used by the APM. To obtain b_J magnitudes we first convert the R-band magnitudes from SExtractor's BEST_MAG to total magnitudes. The correction factor, $R_{tot} =$ BEST_MAG $- 0.021 \pm 0.010$, is calculated from the median magnitude difference between SExtrator's BEST_MAG magnitude and a large (15″ diameter) aperture magnitude for isolated sources. The correction is applied to all sources to convert their BEST_MAG magnitudes to true total magnitudes. Next, we convert these total R-band magnitudes, R_{tot}, to total B-band magnitudes (B_{tot}) using $B_{tot} = R_{tot} + (B - R)$, where $(B - R)$ is the colour measured from the seeing-matched tiles in a 4″-diameter aperture.
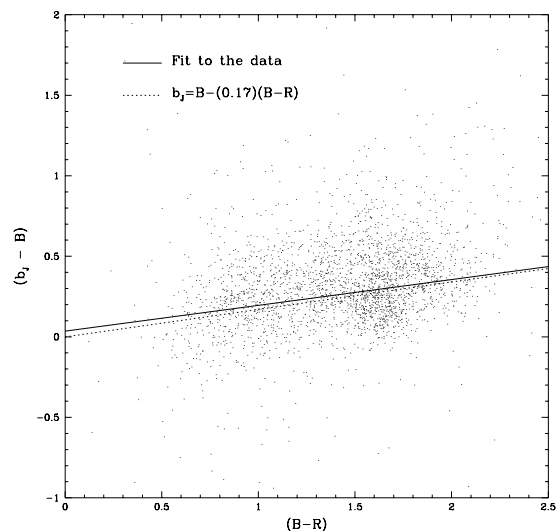
The APM uses photographic b_J magnitudes, and we

Figure 4. Plot of the correlation between (b_J-B) and (B-R) colour for sources from LARCS that are matched to the APM. The solid line is the best fit to the data points. The dotted line is the derived theoretical line $b_J = B - (0.17)(B - R)$. The theoretical line is consistent with the fitted line.

therefore require a colour transformation to convert our CCD-based Johnson B-band magnitude into b_J. Metcalfe et al. (1995) and a number of other authors, including Colless (1989) and Bardelli et al. (1998), provide conversions from B to b_J: $b_J = B - (0.28 \pm 0.04)(B - V)$. From fitting the predicted colours of galaxies across the range of redshift covered by the LARCS clusters with non-evolving spectral energy distributions, we derive the relation between $(B - V)$ and $(B - R)$ to be $(B - R) = (1.66 \pm 0.03)(B - V)$. Hence to convert from the B magnitudes used in LARCS to the b_J APM magnitudes, we use $b_J = B - (0.17 \pm 0.05)(B - R)$. This conversion is consistent with the correlation between $B - b_J$ and $(B - R)$ colour found for matched sources between the APM and LARCS data (see Figure 4), where the calculated fit is $b_J = B - (0.16 \pm 0.03)(B - R) + (0.04 \pm 0.02)$.

In our comparison we use corrected (i.e. including a correction for galactic extinction, Schlegel et al. (1998)) b_J magnitudes from the APM and corrected total B-band mag-
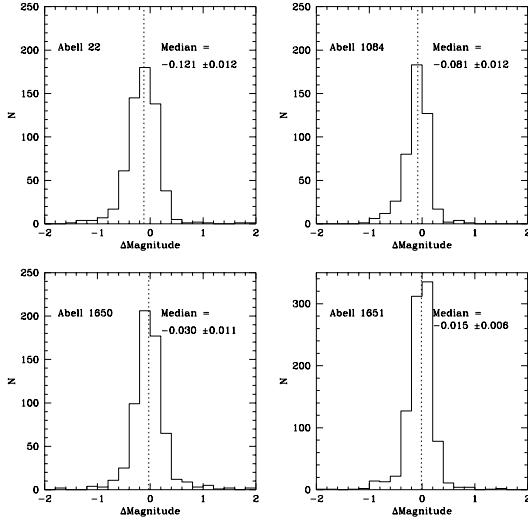
Figure 5. Histograms of the difference between APM magnitude and LARCS total b_J magnitude (the latter converted from B-band) for all four clusters using the full LARCS catalogues. Abell 22 lies in the SGP, the other three are in the NGP. The median magnitude offsets and associated 1σ errors are noted on the individual panels.

Figure 6. Difference in magnitude between LARCS and the APM as a function of LARCS magnitude. The solid line is a fit to those data points brighter than the median magnitude ($b_J^{LARCS} = 18.4$) so as to avoid the selection limit of the GRS/APM (long dashed line). The dotted line represents the $\pm 1\sigma$ limit of this fit. The RMS scatter (long dashed line) ranges from 0.18–0.25, confirming the original estimate of 0.2 made by Maddox et al (1990a).

nitudes from LARCS, converted to b_J. Differences in the magnitudes of matched sources are examined as functions of LARCS mosaic pointing and magnitude.

Figure 5 shows the difference between LARCS b_J and the total APM b_J magnitude for each of the four clusters. The medians and the associated errors are also indicated on the panels. Based on repeat scans of the plate material, Maddox et al. (1990a) suggest an intrinsic uncertainty in the zeropoint of individual plates of 0.04 mag. Of the four clusters, Abell 1650 and Abell 1651 show very good agreement between the two photometric systems, Abell 1084 shows a larger offset (but only at the $\sim 2.5\sigma$ level), while Abell 22 has a $\sim 3\sigma$ difference ($\Delta = 0.12$ mags). We note that Abell 22 is the only one of the four clusters which falls in the SGP area of the GRS/APM.

We next investigate the precision of individual galaxy measurements. Maddox et al. (1990a) and Folkes et al. (1999) state that the random error associated with the b_J magnitudes is ± 0.2 mag for the range $17.0 \leq b_J \leq 19.45$. In Figure 6 we plot the magnitude difference in b_J between LARCS and the APM galaxies against LARCS magnitude. Excluding regions of the plot close to the selection limits, we find that the fit is consistent with a slope of zero, hence the APM demonstrates a linear photometric scale over at least the range $17 < b_J < 19$. The RMS scatter is also consistent with the random error previously stated by Maddox et al (1990a).

In summary, therefore, we see slight evidence for systematic variations in the zero points of the GRS/APM and LARCS photometry across the four clusters, but such variations are within the limit imposed by the combined errors on the GRS/APM and LARCS zero points and thus are not significant. We also find no evidence for systematic variations between the photometry of the SGP and NGP regions
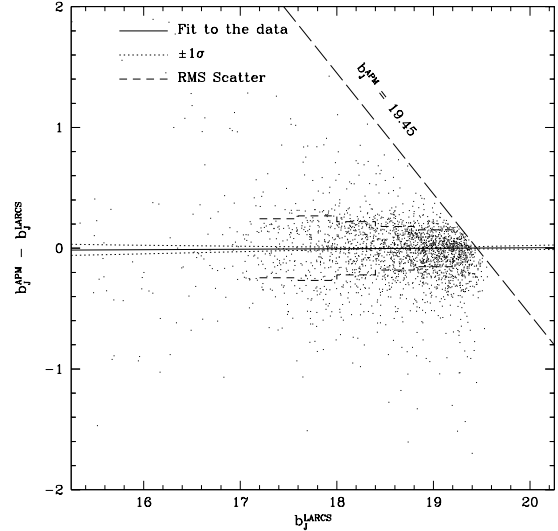
of the GRS/APM at levels $\gg 0.1$ mag. We further note that there is no evidence for a magnitude offset between individual pointings of the mosaic tiles within LARCS at the level of > 0.02 mags (consistent with the photometric errors on the sources used in the comparison).

4 COMPARISON OF THE LARCS GALAXY CATALOGUE WITH THE GRS/APM

We now compare the LARCS and GRS/APM catalogues in the reverse sense: that is we construct a "complete" galaxy catalogue from LARCS and determine the overlap with the GRS/APM.

Because the faint magnitude limit of the GRS/APM input catalogue is $b_J = 19.45$, we generate a bright LARCS sample for each of the four clusters. As we confirmed in §3.2, the typical photometric errors for galaxies in the GRS/APM is 0.2 mag. To ensure the most complete comparison therefore we select all sources from the LARCS catalogues which are at least 3σ (0.6 mag) away from the limit of the GRS/APM: $b_J = 19.45$. This imposes a magnitude limit of $b_J = 18.85$ and we list the number of sources in each field in this "bright" sample in Table 5. Our bright comparison is thus well above the completeness limit and the random scattering of sources above/below the cut-off used for the GRS/APM catalogue. Based upon the scatter at brighter magnitudes (see Figure 6) selecting our sample at $b_J = 18.85$ should exclude at most ~ 3 percent of the population. We further apply our conservative galaxy selection criteria (see §2) to the catalogues to create bright galaxy catalogues for comparison to the GRS/APM input catalogue.

In principle, *all* of the galaxies contained within these

Table 5. Comparison of the bright LARCS catalogues with the GRS/APM catalogue. N(Bright) is the number of sources within the LARCS catalogues when cut at $b_J \lesssim 18.85$. N(Matched) is the number of these LARCS sources matched to the GRS/APM catalogue. N(Galaxies, Matched) is the number of matched galaxies that fall within our stringent star-galaxy separation criteria, whilst N(Galaxies, Unmatched) is the number of unmatched galaxies. See §4 for a full discussion.

Cluster	N(Bright)	N(Matched)	N(Galaxies, Matched)	N(Galaxies, Unmatched)
Abell 22	1997	249	226	35
Abell 1084	2904	177	152	29
Abell 1650	3016	328	249	35
Abell 1651	3521	471	381	70
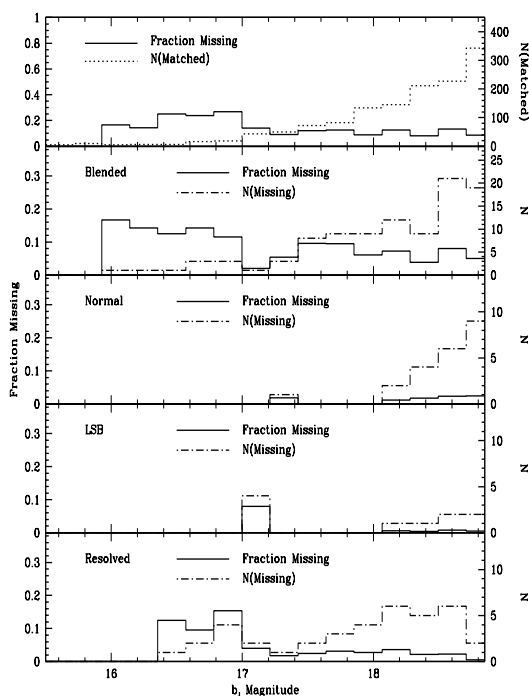
Figure 7. The fraction of bright LARCS galaxies missing from the GRS/APM as a function of b_J magnitude. The top panel shows the total fraction that is missing with the total number of matched galaxies. About 10–20 percent of all galaxies are missed at all magnitudes. The four lower panels break down the missing population into the four broad constituent types. The normal and LSB populations are primarily missed at $b_J > 18.0$, but the blended population is missed across the magnitude range. See §4.2 for discussion.

bright LARCS galaxy catalogues should be present in the GRS/APM. Again, we employ a search radius of $3''$ for the matching algorithm and we give a summary of the results in Table 5.

The GRS/APM identifies the majority of the galaxies contained within the bright LARCS galaxy sample. However, the GRS/APM is missing 10–20 percent of the galaxies at all magnitudes: Figure 7 presents a distribution of the percentage of bright galaxies missing from the GRS/APM

as a function of b_J magnitude, overlaid with the total number of matched galaxies. The missing population represents approximately a fixed fraction of the total population across the whole magnitude range.

To investigate the properties of the missing galaxy population we compare the characteristics of the matched and unmatched galaxies in terms of their morphologies, brightnesses, spatial distributions and $(B - R)$ colours.

4.1 Morphologies of the Missing Populations

Figure 8 shows the distribution of maximum surface brightness (μ_{MAX}) versus concentration index for the matched and missing populations; late-types typically lie towards lower right and early-types populate the upper left of this plane (Abraham et al. 1994). Figure 8 demonstrates that, whilst the missing galaxy population broadly follows that of the matched population, there exist distinct classes of galaxies that are missed in the GRS/APM.

Figure 9 displays a sample of some of these bright galaxies missed from the GRS/APM. We visually classify the unmatched galaxies and define four broad classes absent from the GRS/APM:

- Blends. There are many examples of blended galaxies (see the top two rows of Figure 9). Due to the proximity of a close neighbour or neighbours (either other galaxies or stars), the galaxy is excluded from the GRS/APM catalogue.
- Resolved. There are several apparently 'normal', resolved galaxies missing from the GRS/APM (see the third and fourth rows of Figure 9).
- Normal. There are also small, mostly compact, galaxies which have been missed, the bulk of these are likely to be mis-classified as stellar in the APM and missed from the galaxy survey input catalogue (see the penultimate row of Figure 9).
- LSB. There are a small number of low surface brightness galaxies (see the bottom row of Figure 9).

Blends are the dominant component of the missing galaxy population, comprising 60 percent of it, resolved galaxies 20 percent, normal galaxies 15 percent and low surface brightness galaxies 5 percent (see Table 6).

The majority of the missing population are galaxies blended with a secondary source; both with galaxies (e.g. a1084r09_1155 in Figure 9) and stars (e.g. a22r13_839). In one or both of the APM passbands
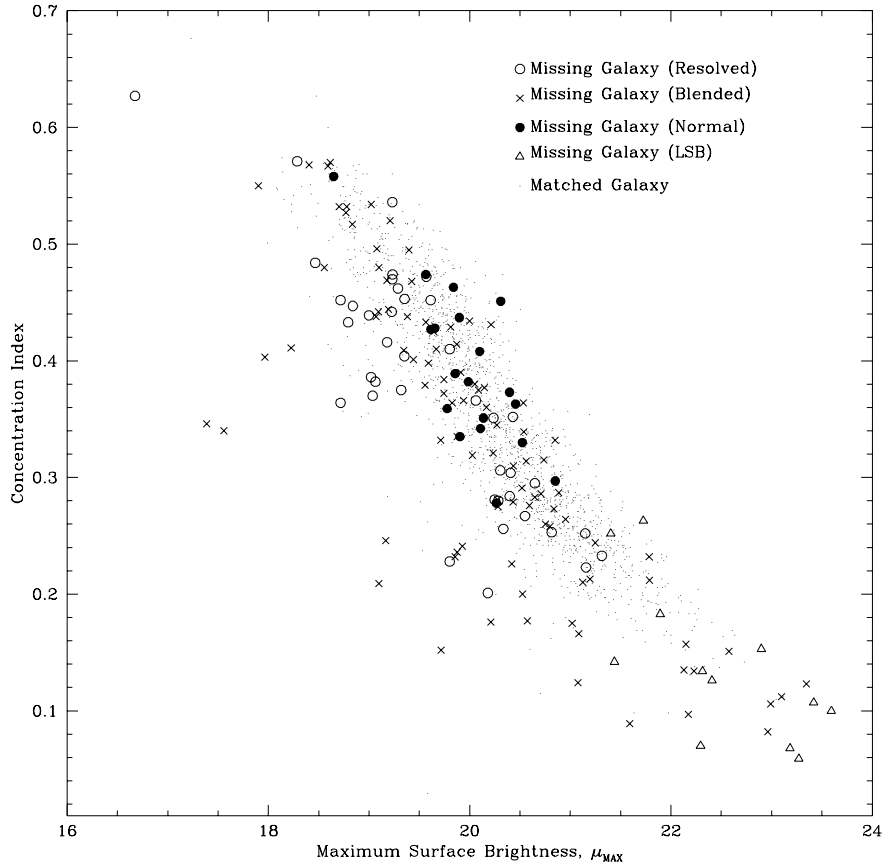
Figure 8. Peak surface brightness, μ_{MAX}, versus concentration index (from SExtractor) for the missing galaxies and the matched sources (dots). The missing population broadly traces the matched population save for the LSBs, which preferentially lie to the lower-right.

Table 6. Breakdown of the morphologies of the bright ($b_J < 18.85$) 'missing' galaxy population obtained from visual inspection of the LARCS CCD material. N(Missing) is the total number of missing galaxies from the GRS/APM. N(Blended) is the number of galaxies that are blended or have a close companion and thus do not appear as distinct sources in the APM. N(Resolved) is the number of apparently normal, resolved galaxies missing from the GRS/APM. N(Normal) is the number of small, often compact, normal galaxies (also see Drinkwater et al. 1999). These galaxies are mis-classified as stellar in the APM. N(LSB) is the number of low surface brightness galaxies missed by the GRS/APM. Several examples of each type of missing galaxy are presented in Figure 9.

Cluster	N(Missing)	N(Blended)	N(Resolved)	N(Normal)	N(LSB)
Abell 22	35	22	5	6	2
Abell 1084	29	17	10	1	1
Abell 1650	35	18	8	4	4
Abell 1651	70	42	16	7	5

(http://www.ast.cam.ac.uk/~apmcat/) these blends have a MERGED flag set. Moreover, as the APM data are scanned from many different plates, the plate quality varies from cluster to cluster. In principle, the plates should be of top quality, but subjective grading of plate quality and variable focus would cause the median separation between blended sources to vary and hence affect the success of deblending. Table 7 presents the median separation of the missing,

merged galaxies. Clearly there are differences in plate quality (and hence the deblending) across the APM, with one plate (containing Abell 1084) having a significantly smaller median blend offset than other plates and the fewest number of blends.

There exists a number of apparently 'normal', resolved galaxies that the GRS/APM misses (e.g. a22r03_1196). These account for $\sim$ 20 percent of the missing pop-
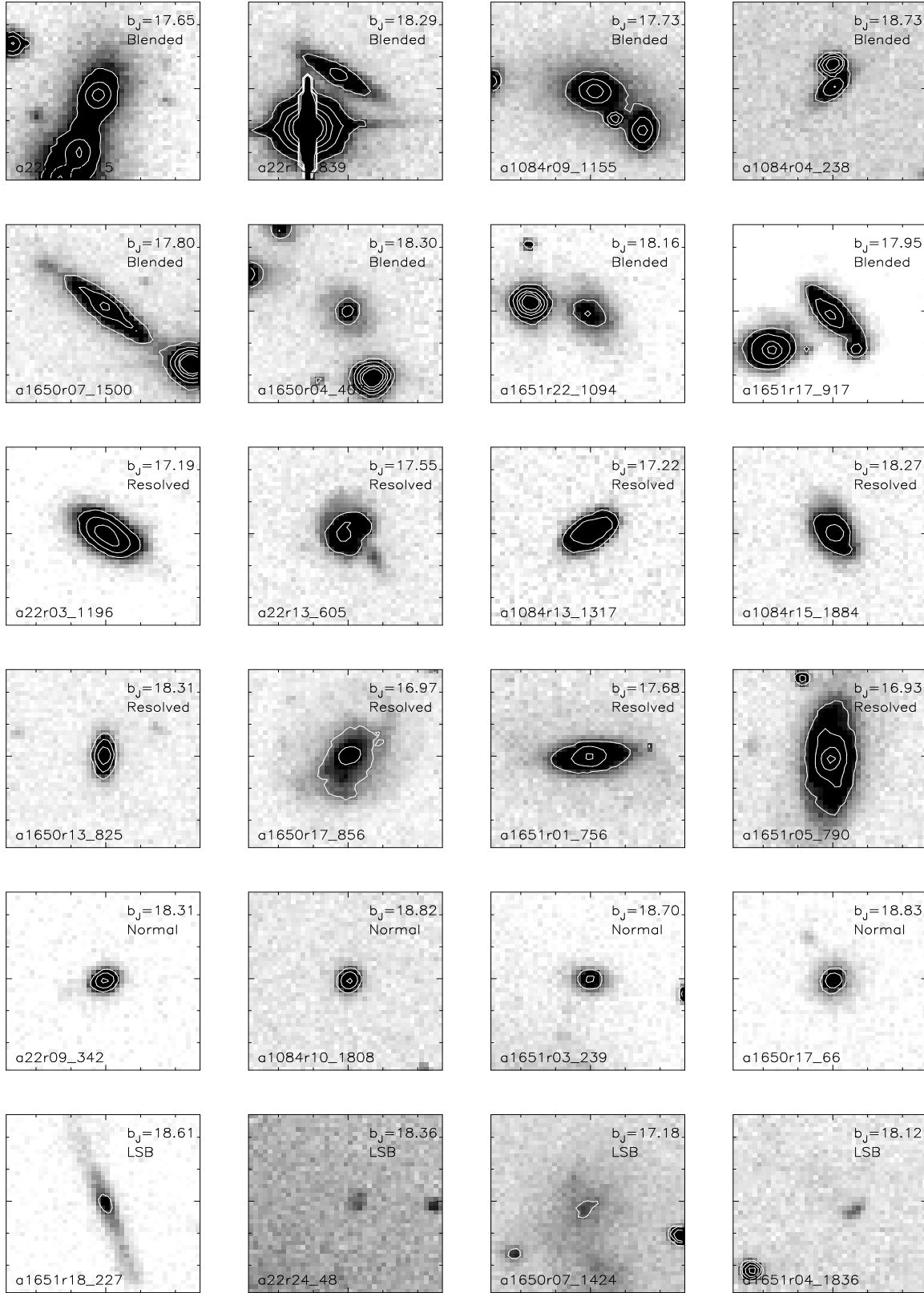
Figure 9. Examples of galaxies missing from the GRS/APM catalogue that appear in the bright ($b_J < 18.85$) LARCS galaxy catalogues. (See §4 and Table 6 for details of the bright comparison). Each box is $30''$ on the side with tickmarks every $5''$. The contours start at a level of $\mu_B = 22$ mag. arcsec^{-2} and increase in brightness by 1 mag arcsec^{-2}. The upper two rows are examples of blended galaxies near stars and other galaxies. The next two rows are normal looking, resolved galaxies incorrectly classified in the APM as not 'non-stellar' in one or both APM passbands. The penultimate row are normal galaxies, classified as stars in the APM. The last row are low surface brightness galaxies.

Table 7. Median distance between the two closest neighbours in a merged source with bootstrap estimates of the 1σ errors. These results may be indicative of varying success of deblending in the APM.

Cluster	Median Merger Distance ($''$)
Abell 22	8.59 ± 0.85
Abell 1084	5.34 ± 0.88
Abell 1650	7.28 ± 0.65
Abell 1651	7.49 ± 0.53

ulations. We investigate these resolved galaxies by inspecting them in the online APM catalogues (see http://www.ast.cam.ac.uk/~apmcat). The Resolved galaxies have classification flags set in one or both passbands to 'noise', 'merged' or 'stellar' (e.g. a1651r05_790 has classification flags set to 'non-stellar' and 'stellar' in the B and R-scans of the APM).

Whilst issues of blending account for ~ 60 percent of the missing APM galaxies, ~ 15 percent of the remainder are bright and relatively compact in nature. With the poorer resolution of the APM, these galaxies are likely to be classified as stellar and indeed most are typed as 'stellar' according to their classification flag in the APM catalogues (e.g. a1084r03_50 has classification flags in both passbands set to 'stellar'). Drinkwater et al. (1999) found evidence for a similar population of small, high surface brightness, compact galaxies within the Fornax cluster. They argue that such galaxies are readily overlooked in many surveys because they are simply misclassified as stars. We confirm that the GRS/APM is systematically missing these compact galaxies from the galaxy catalogue.

The remaining ~ 5 percent of the missing galaxies are low surface brightness systems (LSB). The few examples of the LSB class that are found at all in the on-line APM catalogues are classified as 'noisy', but the majority are missing (e.g. a1651r18_227 has classification flags set to both 'noise-like' and 'merged' in the red and blue APM passbands respectively). Cross et al. (2000) present the bivariate brightness distribution (BBD) for the 2dFGRS survey, which confirms that the majority of these LSB galaxies found in LARCS are outside 2dFGRS's detection limits in surface brightness.

4.2 Magnitude Distribution of the Missing Populations

The missing galaxies appear to be a fixed fraction, about 10–20 percent, of the total population at all magnitudes (see Figure 7, upper panel). The proportion of missing galaxies at the brightest magnitudes, $b_J < 17$, increases to 20 per cent.

Because the missing Blended population dominates the total missing population number, these objects exhibit the same behaviour as the whole missing population across the entire magnitude range. There is no strong dependence on brightness when galaxies are lost from the GRS/APM due to blending.
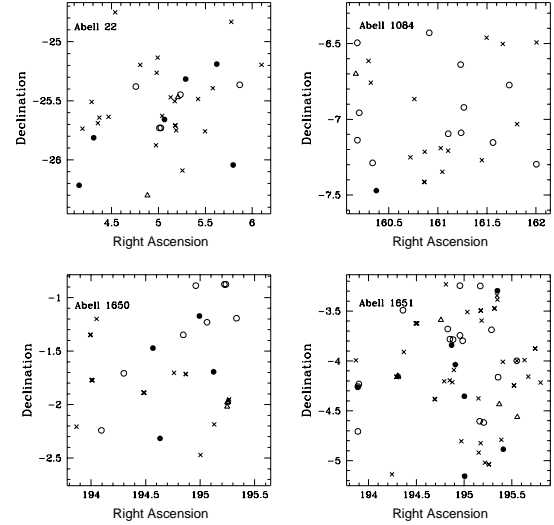

Figure 10. The spatial distribution of the galaxy populations missing from the GRS/APM. Each sub-population, Blends (crosses), Compact (solid circles), Normal (open circles) and LSBs (open triangles) is scattered throughout the two degree fields, with only a slight over-density towards the centre of the cluster (located in the centre of each plot). As Figure 11 shows, the over-density simply reflects the higher proportion of galaxies present in the cluster core.

The missing Resolved galaxies occur more frequently at brighter magnitudes, with few if any fainter than $b_J \sim 18.7$. Many of these brighter normal galaxies are misclassified in one or both APM passbands as blends due to slight asymmetries or irregularities in their morphology.

In contrast, the missing Normal and LSB galaxies are primarily found at fainter magnitudes, $b_J > 18$, relatively uniformly distributed between $b_J \sim 18$ and the magnitude limit of the GRS/APM. Each of these two sub-classes makes up about 1–2 percent of the total population at $b_J > 18$ or fainter. The sensitivity limits of the plate material used in the APM survey means that it preferentially misses faint LSBs, but the dominant factor for distinguishing between faint compact galaxies and stars is the spatial resolution of the APM.

4.3 Spatial Distribution of Missing Populations

The spatial distribution of the missing galaxies is presented in Figure 10. The galaxies are spread evenly throughout the four LARCS clusters. We show the radially-averaged distribution of the different missing galaxy classes for the combined sample from the four clusters (Figure 11). We see that the missing galaxies represent a constant fraction of the whole population at all radii. Although it might be expected that in the crowded clusters cores the proportion of blended galaxies missing from the GRS/APM would increase there is no evidence for this.
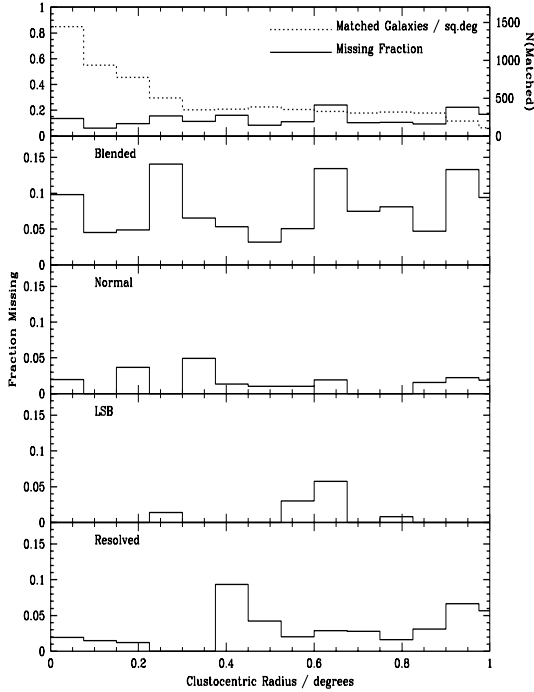
Figure 11. Number of galaxies matched ($b_J \leq 18.85$) per square degree as a function of clustocentric radius, over-plotted with the total fraction of missing galaxies (top panel). The missing populations are approximately a fixed fraction of the total population, which itself decreases with increasing clustocentric distance. The lower four panels illustrate the contribution to the missing fraction for each of the four sub-classes.

Figure 12. The $(B - R)$ colour histograms of the matched and missing galaxy populations, with the missing population subdivided into its various morphological classes. Note the excess of matched galaxies with $(B - R) = 1.6$ – early-type cluster members that account for only around 10 percent of the galaxies in the comparison.

4.4 Colours of the Missing Populations

Histograms of the $(B - R)$ colours of the 'missing' population are presented in Figure 12 together with the colours of the 'matched' population. The excess $(B - R) = 1.6$ galaxies in the matched population are the early-type cluster members; they account for only ~ 10 percent of the galaxies matched in the bright comparison. The missing galaxies span the whole range in colours seen in the matched population, with a slight bias against galaxies with colours similar to early-type galaxies in the clusters and a slightly enhanced number of blue galaxies. The population of Blends dominates the total missing galaxy population. It broadly follows the matched population except for a slight (but not significant) enhancement in the population of very blue galaxies. The Resolved population of missing galaxies traces that of the matched fairly well. Finally, the distributions of missing Normal and LSB galaxies both show shifts to the blue compared to the matched population. This is more pronounced for the missing LSBs, but is still statistically significant for the missing Normal population (likelihood $< 10^{-4}$).

We conclude that the colour biases in some of the populations missing from the GRS/APM are relatively modest as compared to the matched galaxies, especially for the Blended population which dominates the missing sample.
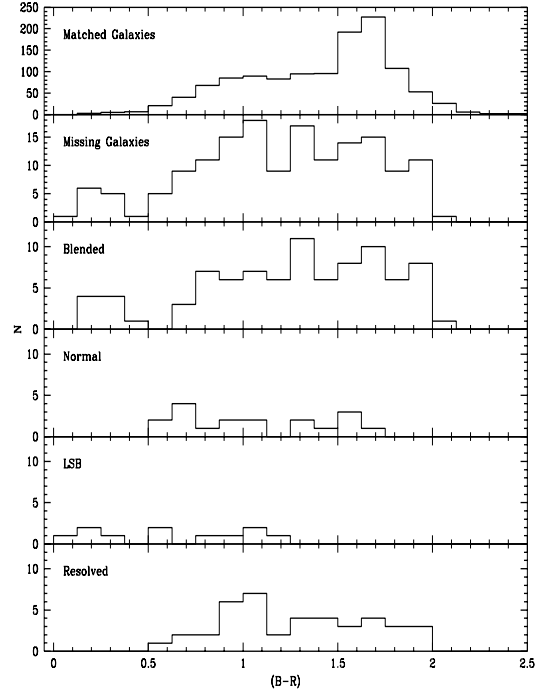
5 CONCLUSIONS

We present the imaging dataset for the Las Campanas and Anglo-Australian Observatories Rich Cluster Survey. This programme is a panoramic CCD-based imaging and spectroscopic study of 21 of the most X-ray luminous clusters of galaxies at $z = 0.07$–0.16. Our imaging extends out to radii of 10 Mpc at the median redshift of our survey–sufficient to encompass the infall region around the clusters. We describe the details of the data reduction pipeline and calibration; our photometry is accurate to ≤ 0.03 mags and our astrometry to better than $0.3''$, as determined from cross-comparisons between overlapping mosaic tiles. We develop a reliable star-galaxy separation technique to provide a low (~ 2 percent) stellar contamination in the final galaxy catalogues.

We compare the results from the LARCS survey for four fields that overlap with the 2dFGRS survey, which is based upon photographic plates scans from the APM. The comparison covers an area ~ 12.3 square degrees on the sky and includes roughly 2500 galaxies brighter than $b_J = 19.45$.

The photometric accuracy of LARCS is accurate to better than 0.03 mag with the internal tile-to-tile photometric match being ≤ 0.005 mag. There is no evidence for a significant offset ($\gg 0.1$mag) between fields in the LARCS survey or between the disconnected regions of the Northern and Southern APM catalogues.

The APM magnitudes are linear across at least two magnitudes in b_J and the random photometrical errors are

found to be consistent with the value of 0.2 mag estimated by Maddox et al (1990a).

The stellar contamination within the GRS/APM is found to be about 3–20 percent, close to the range of 5–10 percent originally estimated by Maddox et al. (1990a).

The number of false detections within the APM is very small, at the ~ 0.1 percent level.

There are several populations of galaxies that are not present within the APM input catalogue: these comprise roughly 10–20 percent of the total galaxy population at all magnitudes. The missing galaxies can be divided in to four broad categories: Blends (60 percent), Resolved galaxies (20 percent), Normal galaxies (15 percent) and Low Surface Brightness galaxies (5 percent).

• The Blends can readily be explained. Due to the resolution of the photographic plates, the APM has not been able to cleanly deblend two sources. As a result these sources are flagged as 'Merged' and removed from the GRS/APM input catalogue. The higher spatial resolution and dynamic range available in the CCD-based LARCS survey allows us to reliably deblend these systems and to investigate the properties of the missing galaxies.

• The missing population of Resolved galaxies has classification flags set in one or both of the APM passbands as stellar, merged or noise. Therefore they are not included in the input catalogue of the 2dFGRS.

• The relatively compact Normal galaxies missing from the GRS/APM input catalogue are classified as stars due to the modest spatial resolution of the plates.

• The Low Surface Brightness galaxies are not present as the APM mostly classifies them as 'noisy' if they are detected. Indeed, the work of Cross et al. (2000) suggests that the majority of them will lie beyond the surface brightness detection limit of the 2dFGRS. These galaxies only represent 5 percent of a magnitude-limited sample and so their absence is less of a concern than the other classes of missing galaxies.

To summarise, the APM input catalogue to the 2dF-GRS survey has a stellar contamination of about 5–10 percent as originally estimated, but misses 10-20 percent of all galaxies at all magnitudes. In terms of their magnitudes, surface brightnesses, colours and compactness, the majority (80 percent of the missing fraction, or ~ 10 percent of the total galaxy population) of these missing galaxies are similar to those included in the GRS/APM and so their absence could be corrected for by simply assuming they represent a random selection of the matched population. However, the remaining 5 percent of the missed galaxy population consists of either LSB or Normal galaxies–these have significantly different properties than the matched population and so their absence cannot be easily corrected for in the 2dFGRS catalogue.

This paper is the first in a series based upon the LARCS survey. Our next paper will focus on the variation in the colours of the cluster population with environment (Pimbblet et al., in prep).

Acknowledgments

REFERENCES

Abraham R.G., Valdes F., Yee H.K.C., van den Bergh S., 1994, ApJ, 432, 75
Bardelli S., Zucca E., Zamorani G., Vettolani G., Scaramella R., 1998, MNRAS, 296, 599
Bertin E., Arnouts S., 1996, A&AS, 117, 393
Cross N., Driver S.P., Couch W.J., et al, 2000 (submitted).
Colless M., 1989, MNRAS, 237, 799
Colless M., 1998, Wide Field Surveys in Cosmology, 14th IAP meeting held May 26-30, 1998, Paris. Publisher: Editions Frontieres. ISBN: 2-8 6332-241-9, p. 77
Drinkwater M.J., Phillipps S., Gregg M.D., Parker Q.A., Smith R.M., Davies J.I., Jones J.B., Sadler E.M., 1999, ApJL, 511, L97
Ebeling H., Voges W., Bohringer H., Edge A.C., Huchra J.P., Briel U.G., 1996, MNRAS, 281, 799 (XBACs)
Folkes S., et al., 1999, MNRAS, 308, 459. (also see http://www.mso.anu.edu.au/2dFGRS/)
Glazebrook K., Peacock J.A., Collins, C.A., Miller L., 1994, MNRAS, 266, 65 (G94)
Kibblewhite E., Bridgeland M., Bunclark P., Cawson M., Irwin M., 1984, IAU Colloq. 78: Astronomy with Schmidt-Type Telescopes, 89
Landolt A.U., 1992, AJ, 104, 372
MacGillivray H.T. & Stobie R.S., 1984, Vistas in Astronomy, 27, 433
Maddox S.J., Efstathiou G., Sutherland W.J., Loveday J., 1990a, MNRAS, 243, 692. (also see http://www.ast.cam.ac.uk/~apmcat/)
Maddox S.J., Efstathiou G., Sutherland W.J., 1990b, MNRAS, 246, 433
Maddox S., et al., 1998, Large Scale Structure: Tracks and Traces, 91
Metcalfe N., Fong R., Shanks T., 1995, MNRAS, 274, 769
O'Hely E., Couch W.J., Smail I., Edge A.C., Zabludoff A., 1998, PASP, 15, 273
O'Hely E., PhD Thesis 'Bridging the gap', UNSW, 2000.
Reid I.N., Yan L., Majewski S., Thompson I., Smail I., 1996, AJ, 112, 1472
Schlegel D.J., Finkbeiner D.P., Davis M., 1998, ApJ, 500, 525